CALCIUM WAVE PROPAGATION BY CALCIUM-INDUCED CALCIUM RELEASE: AN UNUSUAL EXCITABLE SYSTEM

■ JAMES SNEYD
   Department of Biomathematics,
   UCLA School of Medicine,
   10833 Le Conte Ave,
   Los Angeles, CA 90024-1766, U.S.A.

   (*E.mail: jsneyd@biomath.medsch.ucla.edu*)

■ STEVEN GIRARD and DAVID CLAPHAM
   Department of Pharmacology,
   7th floor Guggenheim,
   Mayo Clinic and Foundation,
   Rochester, MN 55905, U.S.A.

We discuss in detail the behaviour of a model, proposed by Goldbeter *et al.* (1990. *Proc. natn. Acad. Sci.* **87**, 1461–1465), for intracellular calcium wave propagation by calcium-induced calcium release, focusing our attention on excitability and the propagation of waves in one spatial dimension. The model with no diffusion behaves like a generic excitable system, and threshold behaviour, excitability and oscillations can be understood within this general framework. However, when diffusion is included, the model no longer behaves like a generic excitable system; the fast and slow variables are not distinct and previous results on excitable systems do not necessarily apply. We consider a piecewise linear simplification of the model, and construct travelling pulse and periodic plane wave solutions to the simplified model. The analogous behaviour in the full model is studied numerically. Goldbeter's model for calcium-induced calcium release is an excitable system of a type not previously studied in detail.

Introduction.   Recently there has been much interest in the spatial and temporal behaviour of calcium (Ca^{2+}) inside cells. Although it has been known for many years that Ca^{2+} is an important intracellular second messenger, the complexity of Ca^{2+} behaviour inside cells has only recently become apparent. In the temporal domain, Ca^{2+} exhibits a wide range of oscillatory behaviour in response to extracellular signals. Dependent on the type of stimulus, the oscillations range from sinusoidal to relaxation type and occur in a variety of non-excitable cells (Cobbold *et al.*, 1991; Harootunian *et al.*, 1991; Petersen *et al.*, 1991; Sauvé *et al.*, 1991: for reviews, see Berridge, 1990; Berridge and Galione, 1988; Tsien and Tsien, 1990; Tsunoda, 1991). Further, the oscillations can be extremely complex with high-frequency oscillations superimposed on higher amplitude, low-

frequency oscillations. It is clear that, to explain thoroughly even the temporal behaviour of Ca^{2+} inside cells, sophisticated models will be necessary.

The behaviour of Ca^{2+} in the spatial domain is also extremely complex. Intracellular and intercellular propagating waves of Ca^{2+} have been observed in a variety of preparations (Berridge, 1990, 1991; Busa and Nuccitelli, 1985; Charles *et al.*, 1991; Gilkey *et al.*, 1978; Sanderson *et al.*, 1990; Thomas *et al.*, 1991), and, using the technique of confocal microscopy, spiral waves, target patterns and plane waves of Ca^{2+} have been observed *in vivo* in the *Xenopus laevis* oocyte (Girard *et al.*, 1992; Lechleiter *et al.*, 1991a,b). It is this experimental data from the *Xenopus* oocyte, demonstrating a wide array of complex spatial behaviours, that stimulates the present work.

There is general agreement as to the initial steps of the process whereby an extracellular signal (agonist) stimulates intracellular Ca^{2+} oscillations. The agonist binds to its receptor and initiates a series of reactions that results in an increased concentration of inositol 1,4,5-trisphosphate (IP_3). IP_3 then causes the release of Ca^{2+} from internal stores resulting in a rise in cytosolic Ca^{2+} concentration (Berridge and Irvine, 1989; Cuthbertson, 1989; Tsunoda, 1991). Although this feed-forward pathway is generally accepted, there is considerable disagreement on the exact nature of the feedback pathway that causes the oscillations and a number of models have been proposed (Cuthbertson and Chay, 1991; Goldbeter *et al.*, 1990; Meyer and Stryer, 1988; Parker and Ivorra, 1990; Swillens and Mercan, 1990; reviewed by Tsien and Tsien, 1990). In general, they fall into two broad categories: (i) models in which oscillations in IP_3 are necessary for oscillations in Ca^{2+}, and (ii) models in which Ca^{2+} oscillations occur independently of IP_3 levels. In the first class of models, the feedback (whether positive or negative) affects the reactions before the formation of IP_3, and in the second class of models, the feedback affects the reactions later in the chain. It is possible that Ca^{2+} oscillations are controlled by different mechanisms in different cells (and thus all the models could well be correct), and probably a number of mechanisms operate simultaneously in some cells, resulting in the complex behaviour described above.

One model that is particularly attractive for modelling regenerative Ca^{2+} release is described by Goldbeter and coworkers (Dupont and Goldbeter, 1989; Dupont *et al.*, 1991; Goldbeter *et al.*, 1990) and involves the mechanism of calcium-induced calcium release (CICR). This mechanism does not require the oscillation of IP_3 to generate Ca^{2+} oscillations and is thus consistent with the evidence from several cells that suggests that oscillations in IP_3 are not necessary for the observed complex spatial behaviour (Girard *et al.*, 1992; Lechleiter *et al.*, 1991a,b). Further, the observed spatial behaviour suggests that positive feedback is important, which is also consistent with Goldbeter's model.

Calcium-induced calcium release was originally proposed as the mechanism governing the excitation–contraction behaviour of cardiac cells and skeletal

muscle fibres (Endo *et al.*, 1970; Fabiato and Fabiato, 1975; Fabiato, 1983), and has since been used in a variety of models (Backx *et al.*, 1989; Cannell and Allen, 1984; Cheer *et al.*, 1987; Kuba and Takeshita, 1981; Lane *et al.*, 1987; Murray and Oster, 1984; Oster and Odell, 1984). However, much of the modelling work is not mathematically rigorous; that which is (the papers by Cheer *et al.*, 1987; Lane *et al.*, 1987; Murray and Oster, 1984) relies on a phenomenological formulation of CICR, rather than a detailed biological construction. A mathematical formulation of CICR, in which the Ca^{2+} dynamics is modelled in more detail, is therefore needed. As we shall show, such a formulation has surprising and interesting consequences.

It is important to note that the present work does not depend on explicit knowledge of the site of CICR. Although it is known that, in some cells, CICR is governed by ryanodine receptors in the endoplasmic or sarcoplasmic reticulum, this is not necessary for the present model. CICR is simply assumed to indicate calcium-sensitive release from some store. This store may or may not be physically distinct from the IP_3-dependent store—the basic structure of the model would remain the same in either case.

We have shown that Goldbeter's model can qualitatively reproduce many of the experimental results obtained from *Xenopus* oocytes. In particular, we have numerically demonstrated the existence of spiral waves, target patterns and plane waves in Goldbeter's model (Girard *et al.*, 1992). Here, we aim towards a better analytical understanding of Goldbeter's model. We show first that Goldbeter's model with no diffusion is analogous to the space-clamped FitzHugh–Nagumo system, and that excitability and oscillations in the model can be understood within the framework of generic excitable system theory. However, when diffusion is added, this convenient analogy breaks down. It is no longer possible to separate the fast and slow variables and previous work on excitable systems does not apply.

It is difficult to gain an intuitive understanding of the behaviour of the model, so, as an aid to this, we consider a piecewise linear approximation to the model. For this approximation, we obtain an analytic expression for the travelling pulse (in one spatial dimension) and show that, as the time scales become widely separated and for a wide range of parameter values, the travelling pulse is unique. We also show that, for each travelling pulse, there is a one-parameter family of periodic wave trains, parameterized by the period, and obtain analytic expressions for these solutions. Further, we show that the travelling pulse is the limit of the periodic plane wave solutions as the period tends to infinity. Analogous results are obtained from the full model by numerical computations.

Temporal Behaviour of the Model.
  The model equations. Goldbeter *et al.* (1990) have presented a set of equations that models CICR and predicts oscillations in Ca^{2+} concentration of

a type similar to those observed in a number of experiments. Although it is clear that there are a number of different mechanisms that control the behaviour of Ca^{2+} inside cells, an understanding of how each mechanism works in isolation is essential for an understanding of Ca^{2+} dynamics *in vivo*. Thus, although CICR is probably not the complete explanation for the observed spatial behaviours in *Xenopus* oocytes, an in-depth analysis of the model will nevertheless prove valuable.

Goldbeter's model is based on the assumption of two functionally distinct internal pools of calcium, called the IP_3-sensitive (S) pool and the IP_3-insensitive (I) pool, respectively. (Detailed presentations of the model have been given by Goldbeter *et al.*, 1990; Berridge, 1989, 1991. We give only a brief description here.) When receptors at the cell membrane are stimulated by an agonist, they initiate a series of reactions, mediated by a G-protein, that results in increased levels of IP_3 in the cytosol. Since IP_3 releases a steady flux of Ca^{2+} into the cytosol from the S pool, an increase in IP_3 concentration results in an increased flux of Ca^{2+} into the cytosol from the S pool. The model assumes that, in the absence of agonist stimulation, there is a small background flux of Ca^{2+} into the cytosol from outside the cell. The Ca^{2+} in the cytosol is sequestered into the I pool, but when the I pool has achieved a high enough level of Ca^{2+} it releases its store back into the cytosol. Hence the phrase, calcium-induced calcium release. Calcium balance is kept by pumps in the cell membrane that pump calcium out of the cell, and the S store is assumed to be kept at a constant concentration by direct interaction with the external medium. A diagram of the calcium fluxes involved in the model is given in Fig. 1. Different cells exhibit varying amounts of I and S pools. The I pool is probably small in *Xenopus* oocytes but larger in neurons. Alternative representations of the model are possible whereby the IP_3-sensitive pool is dominant, but release from it is modulated by the cytoplasmic calcium concentration (Finch *et al.*, 1991; Bezprozvanny *et al.*, 1991; Iino, 1990). Calcium kinetics are assumed to be cooperative and the Ca^{2+} pumps are assumed to be first order. Under these assumptions, the model equations are:

$$\frac{dc_1}{d\tau} = v - kc_1 - \tilde{f}(c_1, c_2)$$

$$\frac{dc_2}{d\tau} = \tilde{f}(c_1, c_2)$$

$$\tilde{f}(c_1, c_2) = \frac{V_1 c_1^n}{K_1^n + c_1^n} - \left(\frac{V_2 c_2^m}{K_2^m + c_2^m}\right)\left(\frac{c_1^p}{K_3^p + c_1^p}\right) - k_f c_2,$$

where c_1 is the concentration of cytosolic calcium, c_2 is the concentration of calcium in the I pool, and τ is time. The function $\tilde{f}$ consists of a series of
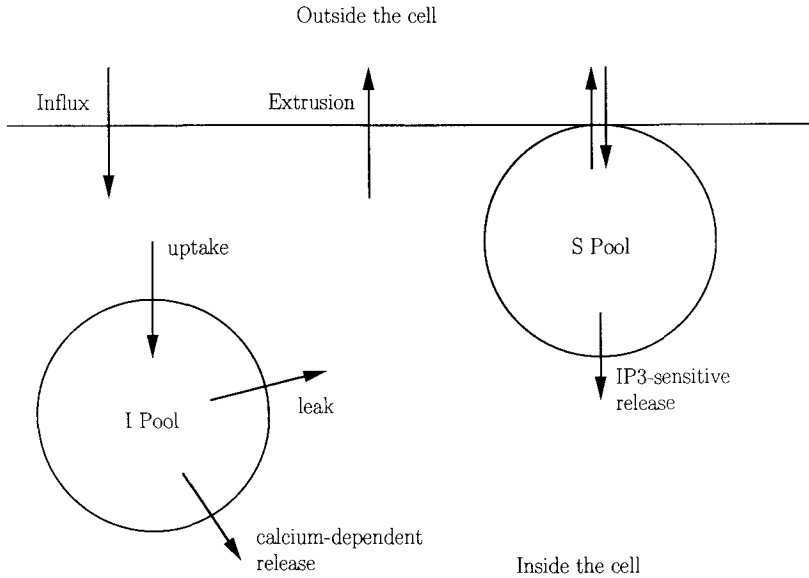
Outside the cell

Figure 1. Simplified diagram of the calcium fluxes and pools involved in the model. For a more detailed presentation of the model see Goldbeter *et al.* (1990).

cooperative kinetic expressions; $V_1 c_1^n/(K_1^n + c_1^n)$ is the rate at which Ca^{2+} is pumped from the cytosol into the I pool, and $\{V_2 c_2^m/(K_2^m + c_2^m)\} \times \{c_1^p/(K_3^p + c_1^p)\}$ is the rate at which it is released through the calcium-dependent release mechanism. Clearly, the second rate depends on both c_1 and c_2; a crucial aspect of this model is the fact that the rate at which Ca^{2+} is pumped from the I pool into the cytosol *increases* as the concentration of Ca^{2+} in the cytosol increases. The constants k and k_f govern the rate at which Ca^{2+} is pumped out of the cytosol and the I pool, respectively, and v governs the rate at which Ca^{2+} is released into the cytosol from the S pool. In general, v will depend on the level of agonist stimulation, and in the model is treated as a bifurcation parameter. When there is no agonist stimulation, v will be the low background Ca^{2+} influx, and agonist stimulation will raise v.

For convenience, we nondimensionalize the equations. Set $u = c_1/K_1$, $v = c_2/K_2$, $t = \tau k$, $\alpha = K_3/K_1$, $\beta = V_1/V_2$, $\gamma = K_2/K_1$, $\delta = k_f K_2/V_2$, $\mu = v/(kK_1)$, $\varepsilon = kK_2/V_2$ to get:

$$\frac{du}{dt} = \mu - u - \frac{\gamma}{\varepsilon} f(u, v) \qquad (1)$$

$$\frac{dv}{dt} = \frac{1}{\varepsilon} f(u, v) \qquad (2)$$

$$f(u, v) = \beta\left(\frac{u^n}{u^n+1}\right) - \left(\frac{u^p}{u^p+\alpha^p}\right)\left(\frac{v^m}{v^m+1}\right) - \delta v. \tag{3}$$

Note that if the kinetics of the exchange of Ca^{2+} between the cytoplasm and the I pool are fast (i.e. V_1 and V_2 are large), ε will be a small parameter. For the values used in this paper, $\varepsilon \approx 0.04$. In the nondimensionalized model equations, μ is treated as the bifurcation parameter.

Equations (1) and (2) actually describe an entire family of models dependent on the particular choice of the exchange function, $f(u, v)$, that describes the dynamics of Ca^{2+} exchange between the cytosol and the internal Ca^{2+} pool. It should therefore be kept in mind that, although we present results here for a particular choice of f, similar results obtain from exchange functions with similar qualitative properties.

Temporal oscillations.   The temporal behaviour of this model has already been well studied (Dupont and Goldbeter, 1989; Dupont *et al.*, 1991; Goldbeter *et al.*, 1990). In this section we merely rederive some already existing results and express them in a convenient form.

The steady state of equations (1)–(3) is given by:

$$u_0 = \mu \tag{4}$$

$$f(\mu, v_0) = 0. \tag{5}$$

The number of steady states depends on the shape of the curve $f(u, v) = 0$, and its intersections with the line $u = \mu$. However, for the particular choice of f that we use, there is only one steady state.

The linear stability of (u_0, v_0) is governed by the roots of the equation:

$$\lambda^2 + \lambda(\gamma f_u/\varepsilon - f_v/\varepsilon + 1) - f_v/\varepsilon = 0. \tag{6}$$

From (3) we see that $f_v < 0$, i.e. as the concentration of Ca^{2+} in the I pool increases, the rate of entry of Ca^{2+} into this pool decreases. It thus follows that the stability of (u_0, v_0) is governed by $\gamma f_u(u_0, v_0)/\varepsilon - f_v(u_0, v_0)/\varepsilon + 1 = H$, say. If $H > 0$ then the steady state is stable and if $H < 0$ it is unstable. Further, as H crosses zero, we get a Hopf bifurcation and the appearance (or disappearance) of small amplitude periodic orbits. Not surprisingly, this stability criterion yields the same result as the Bendixson criterion used by Dupont and Goldbeter (1989).

Thus, to investigate the existence of periodic orbits as the level of agonist stimulation varies (i.e. as μ varies) we plot H vs μ and look for where $H = 0$. Such a plot is given in Fig. 2a. It is clear that a Hopf bifurcation appears twice for this particular choice of exchange function, at μ_1 and μ_2 say. Using the

software package AUTO developed by E. Doedel (Doedel, 1986) we can track this bifurcation; from Fig. 2b we see that the two bifurcation points are connected by a branch of periodic orbits and that, since the Hopf bifurcations are supercritical, the periodic orbits are stable. Numerical solution of the equations confirms this bifurcation diagram.
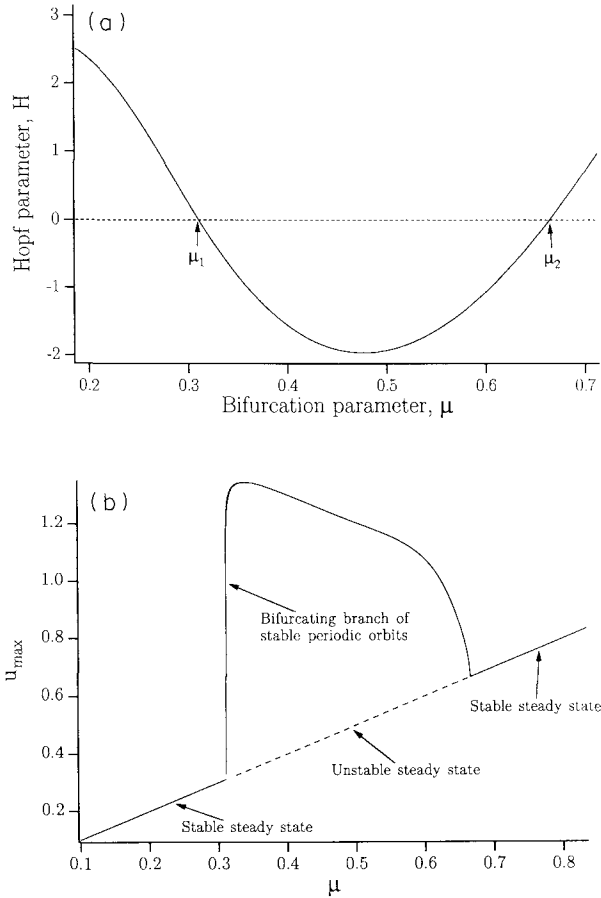

Figure 2. (a) A plot of $H = \gamma f_u/\varepsilon - f_v/\varepsilon + 1$ vs μ. The parameter values used in this figure, and in all the figures in this paper, are $k = 10$ s^{-1}, $K_1 = 1$ μM, $K_2 = 2$ μM, $K_3 = 0.9$ μM, $V_1 = 65$ μM s^{-1}, $V_2 = 500$ μM s^{-1}, $k_f = 1$ s^{-1}, $m = n = 2$ and $p = 4$. Thus, $\alpha = 0.9$, $\beta = 0.13$, $\gamma = 2$, $\delta = 0.004$ and $\varepsilon = 0.04$. Similar behaviour obtains for a wide range of parameter values. As explained in the text, the model with no diffusion [equations (1)–(3)] undergoes a Hopf bifurcation when $H = 0$. For these parameter values there are clearly two Hopf bifurcations. (b) The branch of periodic orbits connecting the Hopf bifurcation points of (a). This curve was computed by the software package AUTO. Direct numerical solution of the equations confirms that the Hopf bifurcations are both supercritical and lead to a branch of stable periodic solutions.

A typical oscillation is shown in Fig. 3, in both the phase plane and the time domain. It is a typical relaxation oscillation, with fast spikes separated by longer latent periods. The structure of the periodic solution in Fig. 3b is revealing. The fast spikes are due to the fast exchange of Ca^{2+} between the cytosol and the internal store. The slower portions of the curve are due to the influx of Ca^{2+} from the IP_3-sensitive store. Over this slow part both u and v are slowly increasing as the cell is "charged" with Ca^{2+} by the IP_3-sensitive store. When a threshold (that depends on the level of Ca^{2+} in the cytosol as well as the level in the Ca^{2+}-sensitive store) is reached, the Ca^{2+}-sensitive store discharges, releasing a large amount of Ca^{2+} into the cytosol, giving the upward phase of the spike. The released Ca^{2+} is quickly taken up again by the Ca^{2+}-sensitive store, resulting in the downward phase of the fast spike, the cell starts to recharge again, and the cycle repeats.

Excitability.   When $\mu < \mu_1$, i.e. before periodic orbits appear, the model exhibits excitable behaviour. Subthreshold perturbations from the steady state return to the steady state, superthreshold perturbations have a large transient excursion before returning to the steady state. Even when oscillations appear, excitability is retained; a superthreshold perturbation will cause a large transient excursion that decays to a stable oscillation. This behaviour is typical of an excitable system, a particularly well-studied example of which is the FitzHugh–Nagumo (FHN) model of the nerve impulse (Britton, 1986; Casten *et al.*, 1975; FitzHugh, 1961, 1969; Hastings, 1974, 1976; McKean, 1970; Rinzel, 1976; Troy, 1976), and generally is the result of widely differing time scales in the model. The relaxation oscillations described in the previous section are also a typical feature of systems with fast and slow time scales.

The present model is no exception. Since ε is a small parameter, it is clear that equations (1) and (2) have a fast and a slow time scale. However, there is no separation of fast and slow variables, as u is both a fast and a slow variable. This is easily remedied.

Let $w = u + \gamma v$ to get the transformed system:

$$\frac{dw}{dt} = \mu - (w - \gamma v) \tag{7}$$

$$\frac{dv}{dt} = \frac{1}{\varepsilon} f(w - \gamma v, v) = \frac{1}{\varepsilon} F(w, v). \tag{8}$$

We now have clearly separated fast and slow variables. The nullclines and a typical solution trajectory are shown in Fig. 4. The nullclines, consisting of an "N-shaped" curve and a straight line, are qualitatively similar to the nullclines of the FHN equations. It is therefore clear that the model will behave like a
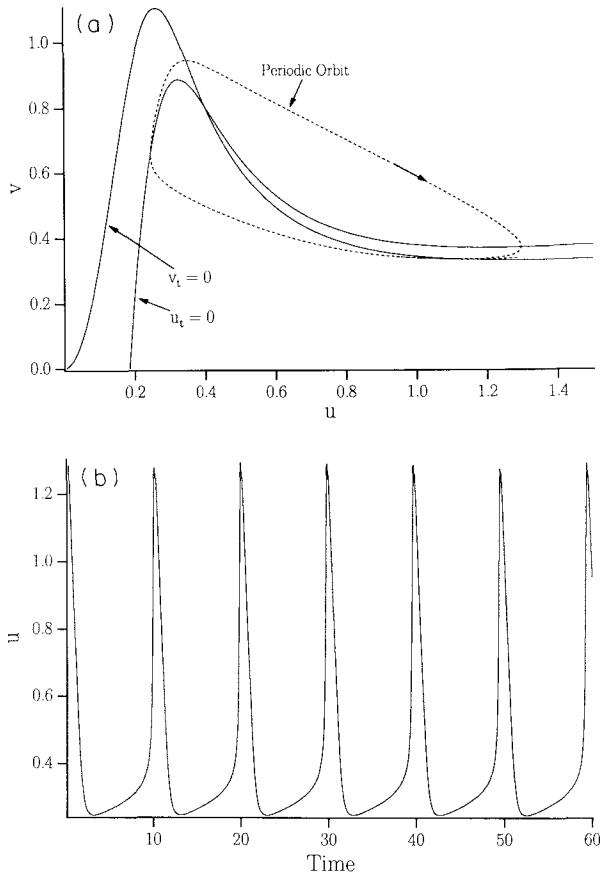
Figure 3. A periodic solution of the model when $\mu = 0.4$. (a) A typical periodic orbit in the u–v phase plane. The nullclines are also shown. (b) The periodic orbit of (a) shown as a function of t. Note the fast spikes separated by longer latent periods. This is typical relaxation oscillation behaviour and is the result of widely differing time scales in the model. A biological interpretation of the periodic orbit is given in the text.

generic excitable system and its temporal behaviour (excitability, the existence of a threshold, the development of oscillations) can be understood by analogy with the FHN equations.

Spatio-temporal Behaviour of the Model.

Introduction. We have shown previously (Girard *et al.*, 1992) that numerical solutions of Goldbeter's model in two spatial dimensions agree qualitatively with experimental observations. All of these computations were performed on the model in the excitable, not the oscillatory regime.

There has been much work done on the spatial behaviour of self-oscillatory systems that are linked by diffusion; it has been shown that periodic plane
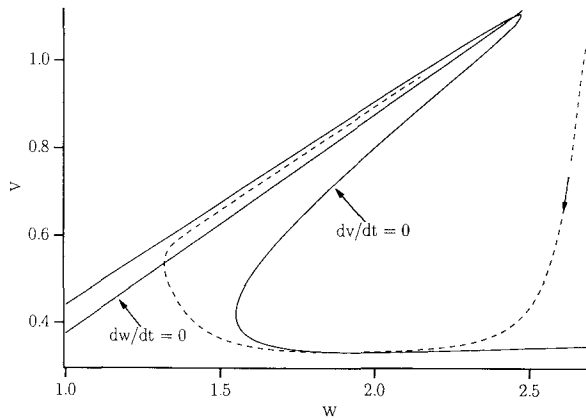
Figure 4. Nullclines and a typical solution trajectory in the transformed phase plane (i.e. *w–v* coordinates). The dotted line is a solution trajectory for $\mu = 0.25$. Note that the nullclines consist of an *N*-shaped curve and a straight line. Hence the behaviour of the model is analogous to the FitzHugh–Nagumo system. With this interpretation, *v* is the fast variable, and *w* is the slow variable.

wave, spiral and pacemaker solutions all exist (Cohen *et al.*, 1978; Duffy *et al.*, 1980; Hagan, 1982; Kopell and Howard, 1973, 1981; Neu, 1979). However, we feel it is unlikely that the observed behaviour is a result of self-oscillatory dynamics. In the first place, the external signal that stimulates the waves is localized to the cell membrane. This signal stimulates oscillations by raising μ past the bifurcation point. Experiments indicate that μ is increased in a region local to the stimulus only, rather than that it is increased homogeneously throughout a large part of the cell. In other words, while the Ca^{2+} dynamics are oscillatory in a localized region of the cell, the remainder of the cell is in a non-oscillatory but excitable regime. The local oscillations are then transmitted to the rest of the cell by the excitable dynamics. This can be tested by measuring the spatial distribution of the stimulus and provides an elegant way of distinguishing between models involving excitability and those involving only self-oscillatory dynamics. In the second place, we have found the spatial behaviour generated by excitability to be considerably more robust than that generated by self-oscillatory dynamics. For these reasons we believe that the observed spatial behaviour is the result of excitable rather than self-oscillatory dynamics. Thus, the excitable nature of the Ca^{2+} dynamics is just as important as the oscillatory behaviour in the transmission of Ca^{2+} signals. The importance of excitability in the transmission of Ca^{2+} signals has not been emphasized in previous studies of the spatial behaviour of Goldbeter's model.

Travelling waves. When diffusion is introduced into the equation for the cytosolic Ca^{2+} (Ca^{2+} in the I store is assumed to be spatially restricted),

appropriate initial conditions stimulate propagating waves of constant amplitude (Fig. 5). However, the simple analogy with the FHN equations breaks down. The model equations with diffusion can be written as:

$$\varepsilon u_t = \varepsilon^2 u_{xx} + \varepsilon(\mu - u) - \gamma f(u, v) \tag{9}$$

$$\varepsilon v_t = f(u, v), \tag{10}$$

where we have rescaled x by $\sqrt{\varepsilon/D}$, D being the diffusion coefficient of cytosolic Ca^{2+}. It is important to note that, due to the presence of the ε in (10) these are *not* the equations of a generic excitable system (Britton, 1986; Keener, 1980, 1986; Murray, 1989), and that, due to the diffusion term, transformation to w, v coordinates does not help. Therefore, previous results on the behaviour of excitable systems cannot necessarily be applied.
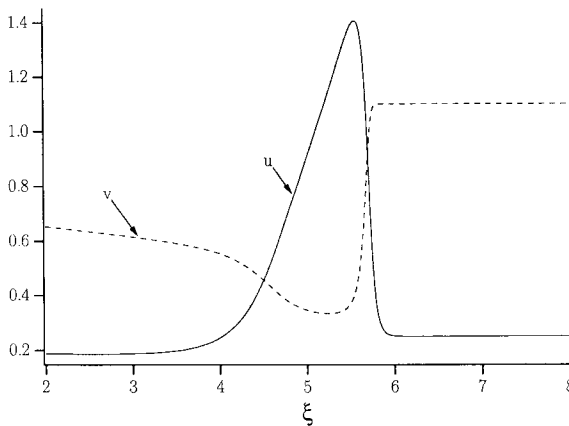

Figure 5. A travelling pulse of the model with diffusion calculated with the NAG library routine D03PGF. Here, $\mu = 0.25$. The pulse is shown here in travelling wave coordinates, and u and v are shown on the same graph. Note the lack of a sharp trailing wavefront.

To look for travelling wave solutions, we transform to travelling wave coordinates, (ξ, t), where $\xi = x + ct$ and c is the speed of the travelling wave, and look for solutions that depend only on ξ. Thus:

$$\varepsilon^2 u'' - \varepsilon c u' + \varepsilon(\mu - u) - \gamma f(u, v) = 0 \tag{11}$$

$$\varepsilon c v' - f(u, v) = 0, \tag{12}$$

where a prime denotes differentiation with respect to ξ. In (u, u', v) phase space, a travelling pulse solution corresponds to a non-constant trajectory that tends to $(u_0, 0, v_0)$ as $t \to \pm \infty$, i.e. a homoclinic trajectory. Such orbits are not easy

to find analytically in three dimensions as phase plane techniques cannot be used. Later, we shall consider the bifurcation diagram of the travelling wave equations, but before we do this, we present a simplified version of the model that helps in our understanding of the full model.

A piecewise linear model.   As an aid to understanding the behaviour of equations (9) and (10) we consider a simpler, piecewise linear model, that retains many of the qualitative features of the full model. This approach was pioneered by McKean (1970) and Rinzel and Keller (1973), who considered a piecewise linear version of the FHN system. The present approach is more similar to the work of Peskin (1976).

We do not linearize the function $f(u, v)$ directly, but instead consider the curve $f(u, v) = 0$. This curve is shown in Fig. 6a. Since, in a qualitative analysis, it is not the actual expression for f that is important but rather the shape of the curve $f = 0$, we replace f by a piecewise linear function, g, such that $g = 0$ approximates the curve $f = 0$. Thus, we replace f by:

$$g(u, v) = \begin{cases} \beta_1 u - v, & u \leqslant a \\ \beta_2 - v, & u > a \end{cases}, \tag{13}$$

where $\beta_1 > 0$, $\beta_2 < 0$ and $a > 0$ are constants. A plot of $g(u, v) = 0$ is given in Fig. 6b. Note that the equations have been shifted so that the steady state is now at $(0, 0)$. Thus, in effect, the constants β_1, β_2 and a depend on the bifurcation parameter μ. The form of the piecewise linear function, g, has a clear biological interpretation. Recall that g is the rate at which Ca^{2+} is transferred from the cytosol to the internal, IP_3-insensitive, pool. Equation (13) just says that: (1) as the concentration of Ca^{2+} in the internal pool increases, the rate of calcium sequestration into that pool decreases; and (2) there is a threshold value of cytosolic calcium concentration $(= a)$ such that, when the concentration reaches the threshold, the calcium flow into the internal pool suddenly reverses and the pool starts to dump its load into the cytosol.

Travelling pulse solution.   We now look for a solution to:

$$\varepsilon^2 u'' - \varepsilon c u' + \varepsilon(\mu - u) - \gamma g(u, v) = 0 \tag{14}$$

$$\varepsilon c v' - g(u, v) = 0 \tag{15}$$

with the form given in Fig. 7. By translating ξ we are able to fix $u(0) = a$, and we also set $u(\xi_1) = a$, where ξ_1 is a constant to be determined. The ξ-axis is thus divided into three regions, in which there are different solutions for u and v: region I, $\xi \leqslant 0$; region II, $0 \leqslant \xi \leqslant \xi_1$; and region III, $\xi_1 \leqslant \xi$. The solutions in the three regions are then joined by continuity and smoothness constraints.
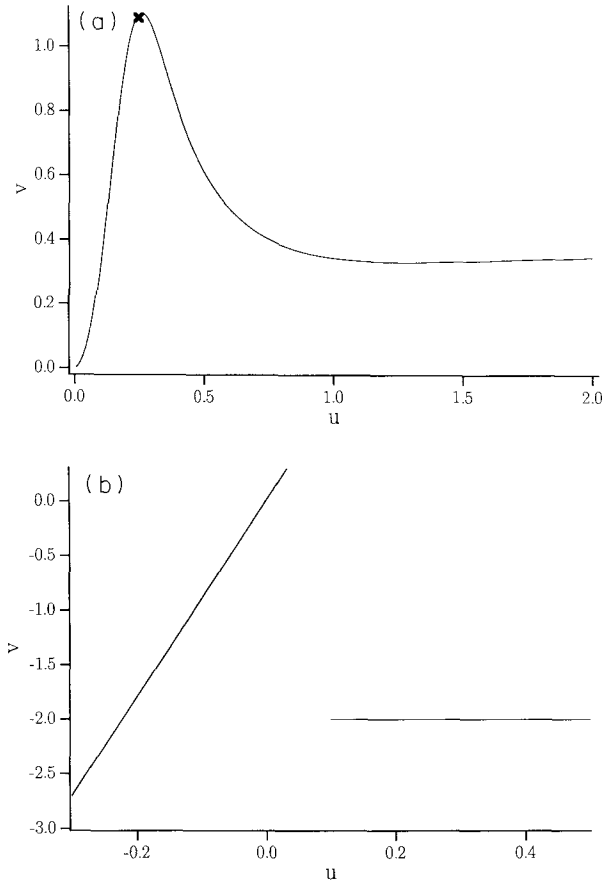
It is easily seen that:

Figure 6. (a) A plot of the curve $f(u, v) = 0$. The steady state for $\mu = 0.25$ (i.e. when the model is in the excitable regime) is shown by the cross. (b) A plot of the curve $g(u, v) = 0$. The function g was chosen so that the curve $g = 0$ is a piecewise linear approximation to the curve $f = 0$, and is used in the construction of a piecewise linear approximation to the model.

$$\left.\begin{array}{l} u_{\mathrm{I}} = A \, \exp(\lambda_3 \xi) \\[2mm] v_{\mathrm{I}} = \dfrac{\beta_1 A}{1 + \varepsilon c \lambda_3} \exp(\lambda_3 \xi) \end{array}\right\}, \xi \leq 0$$

$$\left.\begin{array}{l} u_{\mathrm{II}} = B_2 \, \exp(\lambda_4 \xi) + B_3 \, \exp(\lambda_5 \xi) - \dfrac{\gamma B_1}{1 - \varepsilon + 1/c^2} \exp\!\left(\dfrac{-\xi}{\varepsilon c}\right) \\[4mm] v_{\mathrm{II}} = \beta_2 + B_1 \, \exp\!\left(\dfrac{-\xi}{\varepsilon c}\right) \end{array}\right\}, 0 \leq \xi \leq \xi_1$$
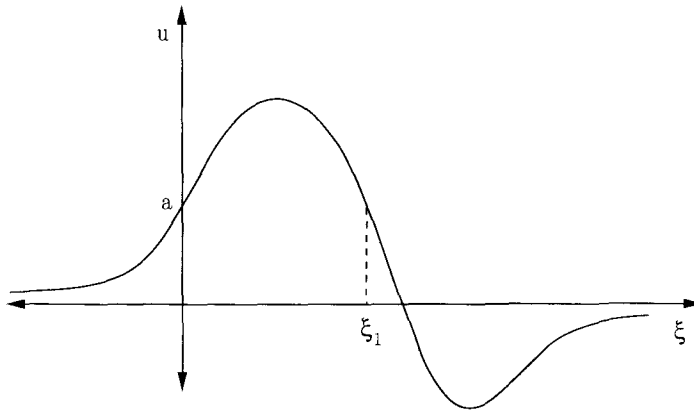
Figure 7. A qualitative picture of a travelling wave of the piecewise linear model, translated so that the steady state is at $u = 0$. Note that $u(0) = a = u(\xi_1)$. This wave is moving from right to left.

$$
\left.
\begin{aligned}
u_{\mathrm{III}} &= D_1 \exp(\lambda_1 \xi) + D_2 \exp(\lambda_2 \xi) \\
v_{\mathrm{III}} &= \frac{\beta_1 D_1}{1 + \varepsilon c \lambda_1} \exp(\lambda_1 \xi) + \frac{\beta_1 D_2}{1 + \varepsilon c \lambda_2} \exp(\lambda_2 \xi)
\end{aligned}
\right\}, \xi_1 \le \xi,
$$

where $A, B_1, B_2, B_3, D_1, D_2, c$ and ξ_1 are constants to be determined, and where we used the fact that the solutions must be bounded at $\pm \infty$. The eigenvalues $\lambda_1 < \lambda_2 < 0 < \lambda_3$ are the roots of:

$$
c \varepsilon^2 \lambda^3 + \varepsilon \lambda^2 (1 - c^2) - \lambda(c + c(\varepsilon + \gamma \beta_1)) - 1 = 0 \tag{16}
$$

and $\lambda_4 < 0 < \lambda_5$ are the roots of:

$$
\varepsilon \lambda^2 - c \lambda - 1 = 0. \tag{17}
$$

Note that, for ε small enough, (16) will have three real roots.

The eight unknown constants are determined from the following constraints.

Continuity:

$$
u_{\mathrm{I}}(0) = u_{\mathrm{II}}(0)
$$
$$
u_{\mathrm{II}}(\xi_1) = u_{\mathrm{III}}(\xi_1)
$$
$$
v_{\mathrm{I}}(0) = v_{\mathrm{II}}(0)
$$
$$
v_{\mathrm{II}}(\xi_1) = v_{\mathrm{III}}(\xi_1).
$$

Consistency:

$$
u_{\mathrm{I}}(0) = a
$$
$$
u_{\mathrm{II}}(\xi_1) = a.
$$

Smoothness:

$$u_I'(0^-) = u_{II}'(0^+)$$

$$u_{II}'(\xi_1^-) = u_{III}'(\xi_1^+).$$

We have constrained v, but not v', to be continuous at 0 and ξ_1, while, since u diffuses, both u and u' are continuous there.

These eight constraint equations result in the following equations for the unknown constants.

Conditions at $\xi = 0$:

$$A = a$$

$$\frac{\beta_1 A}{1 + \varepsilon c \lambda_3} = \beta_2 + B_1$$

$$B_2 + B_3 - \frac{\gamma B_1}{1 - \varepsilon + 1/c^2} = A$$

$$\varepsilon c \lambda_4 B_2 + \varepsilon c \lambda_5 B_3 + \frac{\gamma B_1}{1 - \varepsilon + 1/c^2} = \varepsilon c \lambda_3 A. \tag{18}$$

Conditions at $\xi = \xi_1$:

$$\beta_2 + B_1 \exp\left(\frac{-\xi_1}{\varepsilon c}\right) = \frac{\beta_1 D_1}{1 + \varepsilon c \lambda_1} \exp(\lambda_1 \xi_1) + \frac{\beta_1 D_2}{1 + \varepsilon c \lambda_2} \exp(\lambda_2 \xi_1)$$

$$B_2 \exp(\lambda_4 \xi_1) + B_3 \exp(\lambda_5 \xi_1) - \frac{\gamma B_1}{1 - \varepsilon + 1/c^2} \exp\left(\frac{-\xi_1}{\varepsilon c}\right)$$
$$= D_1 \exp(\lambda_1 \xi_1) + D_2 \exp(\lambda_2 \xi_1)$$

$$D_1 \exp(\lambda_1 \xi_1) + D_2 \exp(\lambda_2 \xi_1) = a$$

$$\lambda_4 B_2 \exp(\lambda_4 \xi_1) + \lambda_5 B_3 \exp(\lambda_5 \xi_1) + \left(\frac{1}{\varepsilon c}\right)\left(\frac{\gamma B_1}{1 - \varepsilon + 1/c^2}\right)\exp\left(\frac{-\xi_1}{\varepsilon c}\right)$$
$$= \lambda_1 D_1 \exp(\lambda_1 \xi_1) + \lambda_2 D_2 \exp(\lambda_2 \xi_1). \tag{19}$$

It is not possible to get an analytic solution to these equations. However, as $\varepsilon \to 0$ the system becomes considerably simpler. In this limit we have:

$$\varepsilon \lambda_1 \to \theta_- = \min\left\{\frac{1 - c^2}{2c} \cdot \left[-1 \pm \sqrt{1 + \frac{4c^2(1 + \gamma \beta_1)}{(1 - c^2)^2}}\,\right]\right\}$$

$$\lambda_2 \to \frac{-1}{c(1 + \gamma \beta_1)}$$

$$\varepsilon\lambda_3 \rightarrow \theta_+ = \max\left\{\frac{1-c^2}{2c}\cdot\left[-1\pm\sqrt{1+\frac{4c^2(1+\gamma\beta_1)}{(1-c^2)^2}}\right]\right\},$$

and

$$\lambda_4 \rightarrow -\frac{1}{c}$$

$$\varepsilon\lambda_5 \rightarrow c.$$

If we assume that (i) $B_3 \rightarrow 0$ and $D_1 \rightarrow \infty$ at such a rate that $B_3 \exp(\lambda_5\xi_1) \rightarrow \bar{B}_3$ and $D_1 \exp(\lambda_1\xi_1) \rightarrow \bar{D}_1$, where $\bar{B}_3$ and $\bar{D}_1$ are constants; and (ii) B_1, c and ξ_1 stay bounded as $\varepsilon \rightarrow 0$ then we get the following simplified system as $\varepsilon \rightarrow 0$. Conditions at $\xi = 0$:

$$A = a$$

$$\frac{\beta_1 a}{1+c\theta_+} = \beta_2 + B_1$$

$$B_2 - \frac{\gamma B_1}{1+1/c^2} = a$$

$$\frac{\gamma B_1}{1+1/c^2} = ac\theta_+. \tag{20}$$

Conditions at $\xi = \xi_1$:

$$\frac{\beta_1 \bar{D}_1}{1+c\theta_-} + \beta_1 D_2 \exp\left(\frac{-\xi_1}{c(1+\gamma\beta_1)}\right) = \beta_2$$

$$B_2 \exp(-\xi_1/c) + \bar{B}_3 = \bar{D}_1 + D_2 \exp\left(\frac{-\xi_1}{c(1+\gamma\beta_1)}\right)$$

$$\bar{D}_1 + D_2 \exp\left(\frac{-\xi_1}{c(1+\gamma\beta_1)}\right) = a$$

$$\theta_+ \bar{B}_3 = \theta_- \bar{D}_1. \tag{21}$$

Equations (20) can be solved to give:

$$\frac{\beta_1 a}{1+c\theta_+} - \beta_2 = \frac{ac\theta_+}{\gamma}\left(1+\frac{1}{c^2}\right), \tag{22}$$

which determines the wave speed, c. Using the fact that $c\theta_+^2 + \theta_+(1-c^2) - c(1+\gamma\beta_1)=0$, we can write (22) in the more convenient form:

$$-\beta_2(1+c\theta_+) = \frac{a}{\gamma}[(c^2+1)(c\theta_+ +1)+c^2\gamma\beta_1].$$

Define:

$$\phi(c) = -\beta_2(1+c\theta_+) - \frac{a}{\gamma}[(c^2+1)(c\theta_+ +1)+c^2\gamma\beta_1].$$

Then, $\phi(0) = -\beta_2 - a/\gamma$ and $\phi \to -\infty$ as $c \to \infty$. Thus, a sufficient condition for at least one positive root is $-\beta_2 - a/\gamma > 0$. A plot of $\phi(c)$ is given in Fig. 8, from which it is easily seen that there is a unique travelling pulse solution for the
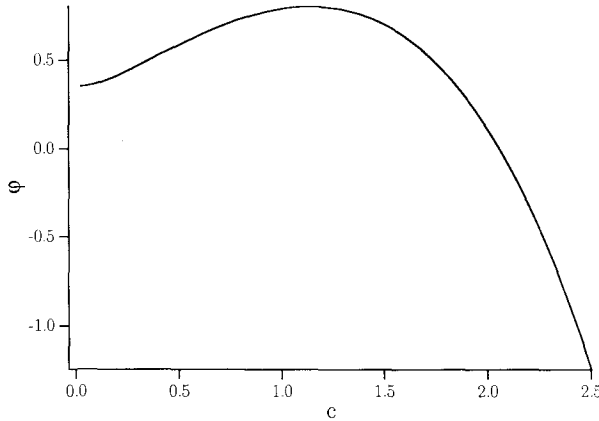

Figure 8. A plot of $\phi(c)$. As $\varepsilon \to 0$ the travelling wave speeds of the piecewise linear model are given by the roots of this equation. We used the parameters, $\beta_1 = 2.6$, $\beta_2 = -0.4$, and $a=0.1$. In this case, there is a unique travelling wave when $\varepsilon = 0$. Similar behaviour was obtained for a range of parameter values.

given parameters. From Fig. 8 it appears that, if $\phi(0) < 0$, there might be two solutions to $\phi(c) = 0$. However, this is not the case, since $\phi(0) \leqslant 0 \Rightarrow \phi(c) < 0$ for all c as can be easily seen. Once c is determined, (20) and (21) are solved for the other constants. The corresponding solution is:

$$u_{\mathrm{I}} = 0$$

$$v_{\mathrm{I}} = 0$$

$$u_{\mathrm{II}} = B_2 \exp(-\xi/c)$$

$$v_{\mathrm{II}} = \beta_2$$

$$u_{\mathrm{III}} = D_2 \exp\left(\frac{-\xi}{c(1+\gamma\beta_1)}\right)$$

$$v_{\mathrm{III}} = \beta_1 D_2 \exp\left(\frac{-\xi}{c(1+\gamma\beta_1)}\right),$$
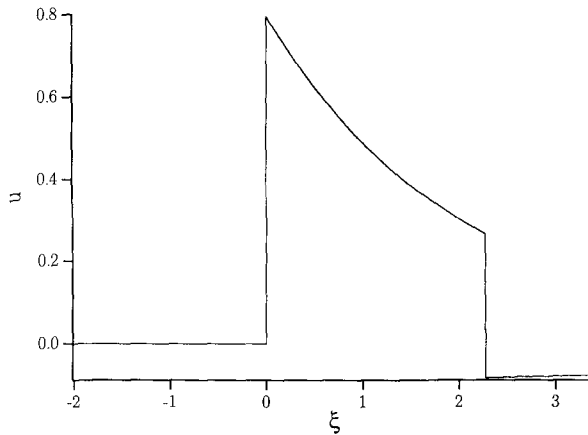
a plot of which is given in Fig. 9.

Figure 9. The travelling pulse solution to the piecewise linear model when $\varepsilon = 0$. Here, $c = 2.06$, $B_1 = 0.43$, $B_2 = 0.8$, $D_2 = -0.1$ and $\xi_1 = 2.27$. The other parameters are as in Fig. 8.

Equations (18) and (19) can be solved numerically for small but non-zero ε, and the corresponding solution is given in Fig. 10. The values for the constants are similar to the values obtained for $\varepsilon = 0$ and the analytic solution agrees well with the solution obtained by direct numerical solution of the differential equations. We were not able to find any other solutions to (18) and (19) which suggests that the uniqueness of the travelling pulse solution when $\varepsilon = 0$ still obtains when ε is small but non-zero.

A plot of wave speed vs a (for $\varepsilon = 0.04$) is given in Fig. 11a. Note that varying a is qualitatively similar to varying μ in the full model: an increase in a corresponds to a decrease in μ. By considering the case $\varepsilon = 0$ this curve may be given a simple intuitive explanation. From the expression for $\phi(0)$ we see that, as a increases, $\phi(0)$ decreases. Noting that, for fixed $c = c_0$, $d\phi(c_0)/da < 0$ it follows that the root of $\phi(c) = 0$ will decrease as a increases. Further, for a large enough, the travelling pulse solution disappears. We therefore expect that, in the full model, as μ decreases, the travelling pulse solution slows down and eventually disappears. This is indeed found numerically; we discuss this behaviour in more detail later.
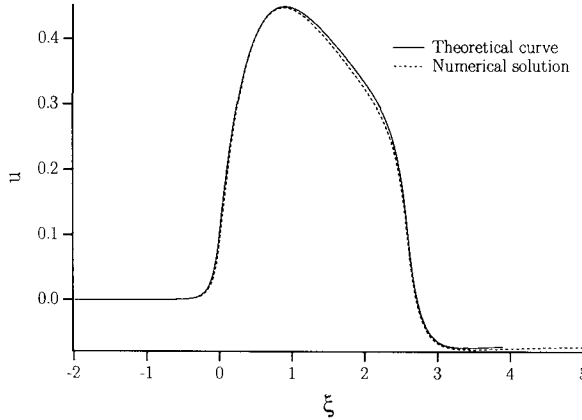
Figure 10. The travelling pulse solution to the piecewise linear model when $\varepsilon = 0.04$. The solid curve was calculated by solving the nonlinear equations (18) and (19) and the dashed curve was calculated by direct solution of the piecewise linear model using forward Euler integration.

Periodic plane wave solutions.   Periodic plane wave solutions are periodic solutions of the travelling wave equations:

$$\varepsilon^2 u'' - \varepsilon cu' + \varepsilon(\mu - u) - \gamma g(u, v) = 0$$

$$\varepsilon cv' - g(u, v) = 0.$$

We can construct such solutions in the same way that we constructed a travelling pulse solution. We look for a periodic solution on $[\xi_1, \xi_2]$, $\xi_1 < 0 < \xi_2$ such that $u \leqslant a$ on $[\xi_1, 0]$ (region I) and $u \geqslant a$ on $[0, \xi_2]$ (region II). The constraints at $\xi = 0$ are:

$$u_\mathrm{I}(0) = a$$

$$u_\mathrm{I}(0) = u_\mathrm{II}(0)$$

$$u'_\mathrm{I}(0^-) = u'_\mathrm{II}(0^+)$$

$$v_\mathrm{I}(0) = v_\mathrm{II}(0)$$

and at the endpoints are:

$$u_\mathrm{I}(\xi_1) = a$$

$$u_\mathrm{I}(\xi_1) = u_\mathrm{II}(\xi_2)$$

$$u'_\mathrm{I}(\xi_1^+) = u'_\mathrm{II}(\xi_2^-)$$
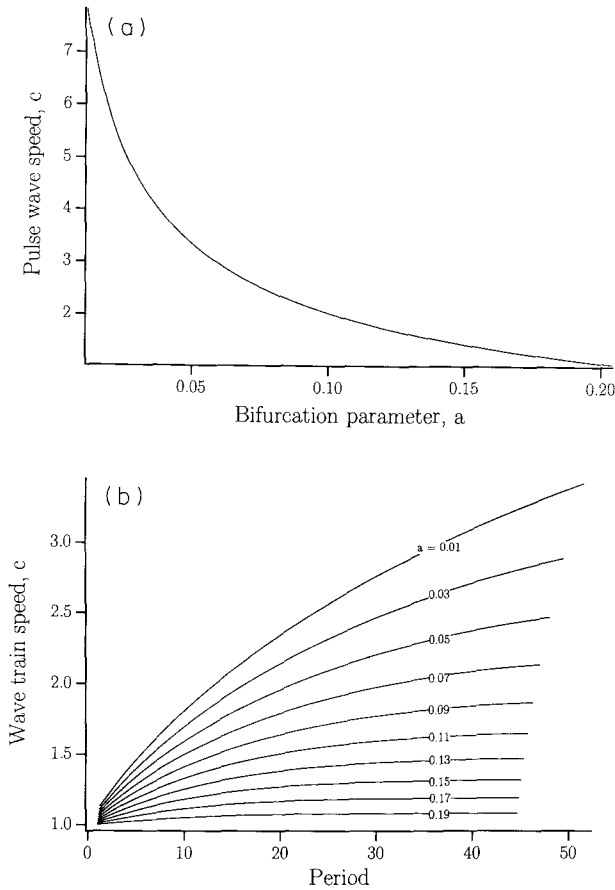
$$v_\mathrm{I}(\xi_1) = v_\mathrm{II}(\xi_2).$$

Figure 11. (a) Speed of the travelling pulse in the piecewise linear model vs a for the case $\varepsilon = 0.04$. As a increases (which is analogous to μ decreasing in the full model), the pulse speed decreases. We expect to see similar behaviour in the full model. This is an important model prediction which should be amenable to experimental verification. (b) Dispersion curves (period *vs* wave speed) for periodic plane wave solutions of the piecewise linear model. For each value of a, as the period tends to infinity, the wave speed tends to the speed of the travelling pulse corresponding to that value of a [given in (a)]. Note that, for fixed c, as the period increases, a increases. Thus we expect that in the full model, for a fixed wave speed, as the period increases, μ decreases. This is indeed found, and is shown in Fig. 13b. From the curves shown here, it appears that, as $T \rightarrow 0$, $c \rightarrow 1$ for each value of a.

We restrict ourselves to looking for periodic solutions of this particular form, as this is consistent with numerical results from the full model. However, periodic solutions of a different form are not necessarily excluded.

We do not give the details here, but it turns out that the differential equations result in nine unknown constants (including c, ξ_1 and ξ_2), to be

determined by the eight constraint equations. For each travelling wave speed, there is a family of periodic plane waves parameterized by the period. Further, we can show that in the limit as $\xi_1 \to -\infty$ with ξ_2 held fixed (i.e. as the period goes to infinity), the periodic solution is just the travelling pulse solution found in the previous section.

Summary of piecewise linear behaviour.   The results of the two previous sections are summarized in Fig. 11. In Fig. 11a, the wave speed of the travelling pulse is plotted against a; an intuitive explanation of the shape of this curve was given before. When $\varepsilon \to 0$ this travelling pulse is unique; when ε is small but non-zero, the travelling wave solution is close to the solution for $\varepsilon = 0$, and appears to be unique. In Fig. 11b, the wave speed of the periodic plane wave solutions is plotted against period, T, for varying values of a. As can be seen by comparing Fig. 11a and b, for each a, as $T \to \infty$, the wave speed tends to the speed of the travelling pulse for that value of a. Further, for a fixed wave speed, c, as T increases, a increases. All of these results can be reproduced in the full model. As yet we have done no analysis on the properties of the dispersion curves as $T \to 0$. Computational results indicate that the dispersion curves for all values of a tend towards 1 as the period becomes small. As yet we have not proved this analytically, and neither have we proved the existence of periodic wave solutions as $T \to 0$. The question of how the dispersion curves begin is the most important question left unanswered in the present work and is discussed further when the dispersion curves for the full model are discussed.

Numerical study of the full model.   Our two principal tools for the numerical study of the full model are the NAG software library subroutine D03PGF, which solves a nonlinear system of parabolic equations by the method of lines and Gear's method, and the software package AUTO for continuation and bifurcation problems (Doedel, 1986).

In the piecewise linear model we saw that, for a fixed value of the bifurcation parameter a, the travelling pulse solution arose as the limit of a one-parameter family of periodic plane waves (parameterized by the period) as the period went to infinity. In the full model, we expect the behaviour to be similar. Thus, although we are ultimately interested in travelling pulse solutions to the full model, we begin by looking for periodic plane wave solutions and then investigate their behaviour as the period becomes large.

Hopf bifurcation to periodic waves.   Periodic plane wave solutions result from a Hopf bifurcation in the travelling wave equations (11) and (12). The linear stability of the critical point is governed by the cubic

$$\lambda^3 - A\lambda^2 - B\lambda + C = 0,$$

where

$$A = \frac{1}{\varepsilon}\left(\frac{f_v}{c} + c\right)$$

$$B = \frac{1}{\varepsilon}H$$

$$C = \frac{f_v}{\varepsilon^2 c}$$

and where

$$H = \frac{\gamma f_u}{\varepsilon} + 1 - \frac{f_v}{\varepsilon}.$$

Note that H is just the Hopf parameter from a previous section (Temporal oscillations), and recall that the model with no diffusion undergoes a Hopf bifurcation when $H = 0$ (cf. Fig. 2).

The conditions for a Hopf bifurcation in the travelling wave equations are (i) $AB = C$ and (ii) $B < 0$. Thus, a Hopf bifurcation can only occur in the travelling wave equations if the ordinary differential equations are in the oscillatory regime, i.e. $H < 0$. Solving the equation $AB = C$ for c gives:

$$c^2 = \frac{-f_v(\gamma f_u/\varepsilon - f_v/\varepsilon)}{H}.$$

The locus of Hopf bifurcation points in the $\mu - c$ plane is shown in Fig. 12 and labelled in the Hopf curve.

Travelling and periodic plane waves.   Included in Fig. 12 is a curve of travelling pulse solutions (solid circles joined by lines), determined by numerical solution of the differential equations. Clearly, as predicted from the piecewise linear model, the speed of the travelling pulse increases as μ increases. Further, for μ small enough, we are unable to find a travelling pulse solution, also as predicted.

Just for now, ignore the open squares in Fig. 12. In order to facilitate understanding of the relationship between the piecewise linear model and the full model, it is helpful to consider what we shall call the dispersion surface. In general, the period of a periodic travelling wave train, T, is a function (not necessarily single-valued) of both the bifurcation parameter, μ, and the speed of the wave train, c. Thus, $T = T(\mu, c)$ can be thought of as a surface in μ, c, T-space, the dispersion surface. The dispersion surface lies above the μ–c plane shown in Fig. 12. By fixing μ, and taking a cross-section of the dispersion surface we obtain the dispersion relation for that value of μ, i.e. c as a function of T for that value of μ (cf. Fig. 14). This is the way the dispersion curve is usually presented. Similarly by fixing c and taking a cross-section of the
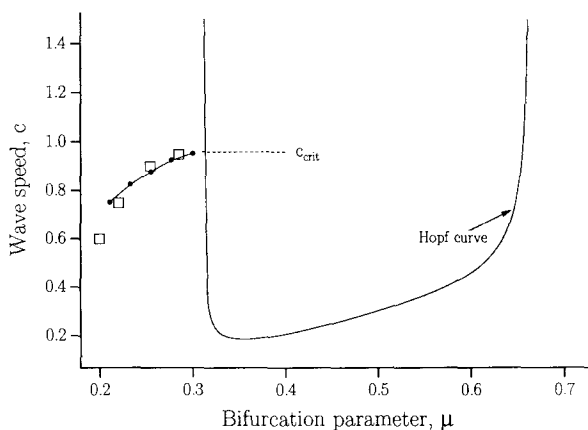
Figure 12. The solid curve (Hopf curve) is the locus of Hopf bifurcation points of the travelling wave equations (11) and (12). At these points we get a bifurcation into periodic plane wave solutions of the model. The solid circles joined by lines are travelling pulse solutions of the full model computed by the NAG subroutine D03PGF. The open squares are approximate travelling pulse solutions computed by AUTO. They are described in more detail in the text and in the caption to Fig. 13. The approximate location of c_{crit} is shown by a dashed line. Computations indicate that c_{crit} is approximately located at the place where the line of travelling pulse solutions (filled circles) intersects the Hopf curve.

dispersion surface we may obtain μ as a function of T for that fixed value of c (cf. Fig. 13). It is clear that the dispersion curve (c vs T) corresponds to taking a "vertical" slice in Fig. 12, while the curve μ vs T corresponds to taking a "horizontal" slice.

To demonstrate the shape of the dispersion surface for the full model we shall present a series of both vertical and horizontal slices, for varying values of μ and c. We do not intend to present an exhaustive and rigorous demonstration of the shape of all branches of the dispersion surface, but merely wish to point out some salient features.

The first point to note is that the line denoted by filled circles (corresponding to a one-parameter family of travelling pulse solutions, parameterized by either μ or c) corresponds to a line of singularities of the dispersion surface; along this line T becomes infinite. Secondly, we reiterate that a Hopf bifurcation to travelling wave solutions occurs along the smooth curve labelled the Hopf curve.

Using AUTO, we can determine the fate of the bifurcating periodic waves. Let c_{crit} denote the value of c where the line of travelling pulse solutions (solid circles, Fig. 12) intersects the Hopf cuve. Here, $c_{crit} \approx 1$. From the numerical results presented in Figs 12 and 13 it appears that, for $c > c_{crit}$, the two Hopf bifurcation points are connected by a branch of periodic orbits (Fig. 13a). For $c > c_{crit}$ there are no travelling pulse solutions. However, for $c < c_{crit}$ the branch
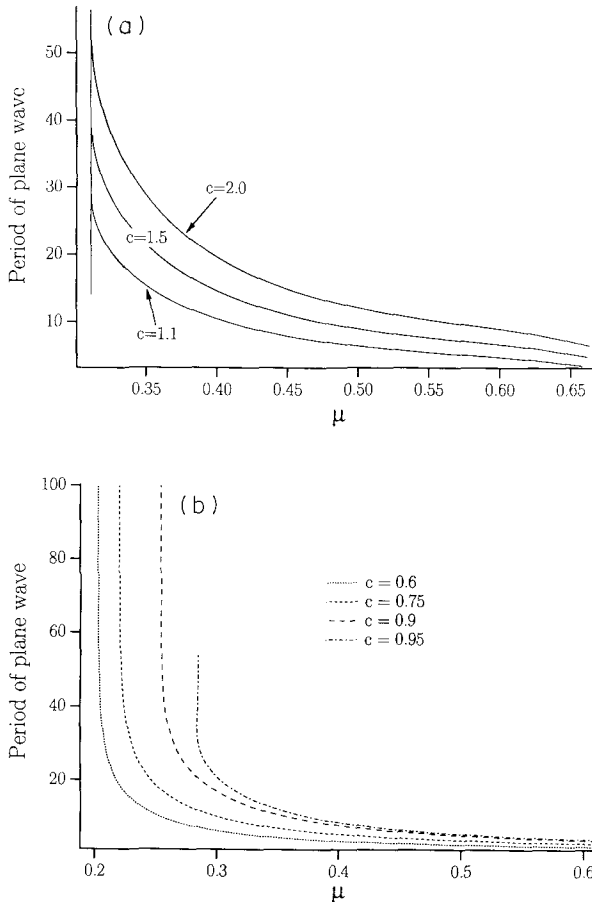
Figure 13. Cross-sections of the dispersion surface for various fixed values of c (i.e. horizontal slices in Fig. 12). (a) When $c > c_{crit}$, the Hopf bifurcation points in the travelling wave equations are connected by a branch of periodic plane wave solutions, as shown here. These branches of periodic orbits connect the right and left branches of the Hopf curve shown in Fig. 12. (b) When $c < c_{crit}$, the branch of periodic plane wave solutions originating at the right branch of the Hopf curve terminates in a wave of infinite period i.e. a travelling pulse, as shown here. These travelling pulses are denoted by open squares in Fig. 12 and correspond to the travelling pulses obtained by direct integration of the equations.

of periodic orbits emanating from the right hand Hopf bifurcation point terminates in a periodic orbit of infinite period, i.e. a travelling pulse, as shown in Fig. 13b. Note that the curves given in Fig. 13a and b correspond to cross-sections of the dispersion surface for fixed c, as described above. Approximate values of c and μ for the infinite period solutions shown in Fig. 13b are shown as open boxes in Fig. 12. They appear to correspond to the previously computed travelling pulse solutions. Hence, just as in the piecewise linear
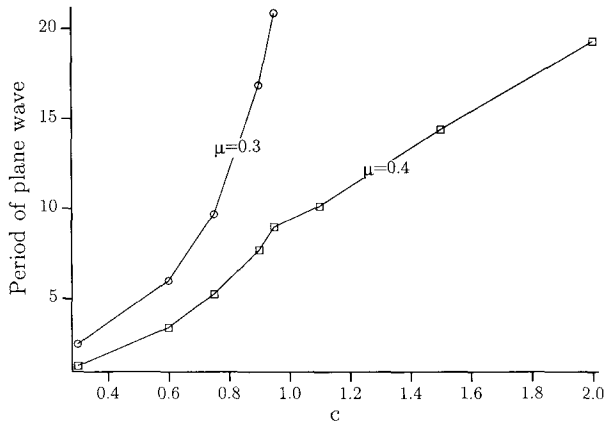
Figure 14. Cross-sections of the dispersion surface for two fixed values of μ; when $\mu = 0.3$ the model is in the excitable regime, and when $\mu = 0.4$ the Hopf bifurcation has been crossed, the steady state is unstable, and the model is oscillatory. The symbols were determined by the intersection of the line $\mu = 0.4$ (or $\mu = 0.3$) with the curves given in Fig. 13. Note that, when $\mu = 0.3$, T becomes infinite at a finite value of c, corresponding to a travelling pulse solution. This travelling pulse solution lies on the line denoted by the filled circles in Fig. 12. When $\mu = 0.4$ no such travelling pulse solution exists and c and T appear to be approximately linearly related. The $\mu = 0.3$ curve for the full model is analogous to the curves in Fig. 11b for the piecewise linear model.

model, the travelling pulse solutions are the limit of a branch of periodic wave trains with fixed wave speed, as the period tends to infinity.

We may also consider vertical slices of the dispersion surface, i.e. cross-sections of the dispersion surface for fixed μ, and two sample curves are given in Fig. 14. For fixed μ out of the oscillatory regime ($\mu = 0.3$), there is a family of periodic wave trains such that, as the period increases, the speed of the wave train also increases, terminating at the travelling pulse solution corresponding to that value of μ. The $\mu = 0.3$ curve in Fig. 14 is analogous to those in Fig. 11b for the piecewise linear model; the behaviour of the two models in this regime is qualitatively similar. For μ within the oscillatory regime ($\mu = 0.4$), the period of the travelling wave increases as the speed increases. The piecewise linear model has no dispersion curve analogous to the $\mu = 0.4$ curve in Fig. 14 as it has no Hopf bifurcation; as a decreases, instead of a Hopf bifurcation occurring, the dispersion relations merely tend to a bounded, increasing curve (cf. Fig. 11b).

We emphasise that this is not meant to be an exhaustive analysis of the dispersion surface. A number of questions yet remain unanswered. Firstly, the dispersion surface probably has more than one branch when $c < c_{\text{crit}}$. The reader will have noticed that, for a fixed $c < c_{\text{crit}}$, we discussed the fate of the branch of periodic waves originating at the right Hopf bifurcation point but did not discuss the behaviour of the branch of periodic waves emanating from the

left Hopf bifurcation point. This left Hopf point probably contributes a second branch to the dispersion surface but as yet we have not studied this branch at all. Secondly, as μ increases, what happens to the line of travelling pulse solutions denoted by the filled circles? We do not know exactly. Numerical computations indicate that the line of travelling pulse solutions terminates when it intersects the Hopf curve (at c_{crit}) but more work is required on this question. Thirdly, it is not clear how the dispersion curve for $\mu = 0.4$ in Fig. 14 terminates as $c \to \infty$. Although it would seem reasonable to postulate that T does not become infinite for finite c (i.e. that travelling pulse solutions do not exist when μ is in the oscillatory regime) we have not checked this. Finally, and perhaps most importantly, it is not clear how the dispersion curves in Fig. 14 begin. By analogy with the piecewise linear model one might expect that, for $\mu = 0.3$, as $T \to 0$, c tends to a nonzero value, but we do not know this for sure. Clearly, a considerable amount of further work on the detailed structure of the dispersion surface is needed in order to answer these questions.

Despite these unanswered questions, we may still conclude that the behaviour of travelling pulse and periodic plane wave solutions in the full model is similar to that in the piecewise linear model, and thus an intuitive understanding of the full model may be obtained by considering the simplified model.

Discussion and Conclusions.   We have shown that Goldbeter's model is an excitable system of a type not previously studied. Although the model with no diffusion behaves analogously to the FitzHugh–Nagumo equations, the behaviour of the spatially dependent model is unexpected and surprising. The behaviour of the full model was shown to be qualitatively similar to that of a piecewise linear simplification of the model. We demonstrated the existence of a travelling pulse in the simplified model and it appears to be unique (although we did not prove that). Further, the travelling pulse is the limit of a family of periodic plane wave solutions as the period tends to infinity. These results differ from those obtained by Rinzel and Keller (1973) for the FHN equation, which has two travelling pulse solutions, one stable and one unstable. We have not analysed the stability of the periodic plane waves in the simplified model. Computations indicate that some of the periodic plane waves are stable but we have not done a detailed investigation.

It is interesting to compare these results with those obtained by Dockery and Keener (1986). These authors have shown that, when the slow variable in the FHN equations is assumed to diffuse with diffusion coefficient D_s, the bifurcation diagram changes qualitatively as D_s increases. When $D_s = 0$ there are two travelling waves, the slower one being unstable; this is the case analysed by Rinzel and Keller (1973). However, as D_s increases, the slow branch of travelling waves may temporarily disappear, resulting in a situation similar to

that described in this paper, with a unique stable travelling wave. A detailed bifurcation analysis of Goldbeter's model as the diffusivity of v varies has not been performed. Given the work of Dockery and Keener, it is possible that such an analysis will demonstrate a greater qualitative similarity between Goldbeter's model and the FHN equations than is presently apparent.

The present analysis is just a realization of the results of Maginu (1985) who has performed a detailed analysis of the bifurcation of periodic travelling waves in a general reaction–diffusion system. Although some of the results presented here are unexpected for an excitable system, they are nonetheless consistent with the general theory.

Preliminary computational results indicate that the model in two spatial dimensions has unexpected properties. As expected, the geometry of the wave front influences the normal speed of propagation, but the usual formula, $N = c - \varepsilon\kappa$, where N is the normal wave speed, κ is the curvature of the wave front, and c is the plane wave speed (Keener, 1986; Zykov, 1980), does not always apply. More work yet remains to be done on this question. If further, more detailed, investigation confirms this surprising property, it will have important implications in the study of biological excitable systems.

In summary, our results indicate that the behaviour of biological excitable systems can not always be completely understood by analogy with the FHN equations. Goldbeter's model, which is plausibly derived from current theories of the mechanisms underlying Ca^{2+} oscillations, exhibits excitable behaviour of a type not previously studied in detail. In the past, mathematical work has concentrated on the behaviour of systems with separate fast and slow variables, and much is known about the behaviour of such systems in the spatial domain. However, Goldbeter's model exhibits excitability in a rather different form. The mathematical study of this excitable system is just as important from a biological viewpoint, but is far less advanced. The present paper makes a start in this direction. Further, the present work, in demonstrating how a more detailed and realistic model has unexpected properties, emphasizes the importance of knowing the physiological details of the system under investigation in the construction of mathematical models. In particular, it will be important to characterize, for each cell type, the contribution of ryanodine, and IP_3 receptor gated calcium pools, the modulation of these receptors by coagonists, the types and regulation of calcium pumps and the buffering of calcium by intracellular elements.

LITERATURE

Backx, P. H., P. P. de Tombe, J. H. K. Van Deen, B. J. M. Mulder and H. E. D. J. ter Keurs. 1989. A model of propagating calcium-induced calcium release mediated by calcium diffusion. *J. gen. Physiol.* **93**, 963–977.

Berridge, M. J. 1989. Cell signalling through cytoplasmic calcium oscillations. In *Cell to Cell Signalling: From Experiment to Theoretical Models*, A. Goldbeter (Ed.), pp. 449–459. London: Academic Press.

Berridge, M. J. 1990. Calcium oscillations. *J. Biol. Chem.* **265**, 9583–9586.

Berridge, M. J. 1991. Cytoplasmic calcium oscillations: a two pool model. *Cell Calcium* **12**, 63–72.

Berridge, J. J. and A. Galione. 1988. Cytosolic calcium oscillators. *FASEB J.* **2**, 3074–3082.

Berridge, M. J. and R. F. Irvine. 1989. Inositol phosphates and cell signalling. *Nature* **341**, 197–205.

Bezprozvanny, I., J. Watras and B. E. Ehrlich. 1991. Bell-shaped calcium-response curves of Ins(1,4,5)P_3-and calcium-gated channels from endoplasmic reticulum of cerebellum. *Nature* **351**, 751–754.

Britton, N. F. 1986. *Reaction–Diffusion Equations and Their Applications to Biology*, London: Academic Press.

Busa, W. B. and R. Nuccitelli. 1985. An elevated free cytosolic Ca^{2+} wave follows fertilization in eggs of the frog, *Xenopus laevis. J. Cell Biol.* **100**, 1325–1329.

Cannell, M. B. and D. G. Allen. 1984. Model of calcium movements during activation in the sarcomere of frog skeletal muscle, *Biophys. J.* **45**, 913–925.

Casten, R. G., H. Cohen and P. A. Lagerstrom. 1975. Perturbation analysis of an approximation to the Hodgkin–Huxley theory. *Q. Appl. Math.* **32**, 365–402.

Charles, A. C., J. E. Merrill, E. R. Dirksen and M. J. Sanderson. 1991. Intercellular signaling in glial cells: calcium waves and oscillations in response to mechanical stimulation and glutamate. *Neuron.* **6**, 983–992.

Cheer, A., J-P. Vincent, R. Nuccitelli and G. Oster. 1987. Cortical activity in vertebrate eggs I: the activation waves. *J. theor. Biol.* **124**, 377–404.

Cobbold, P. H., A. Sanchez-Bueno and C. J. Dixon. 1991. The hepatocyte calcium oscillator. *Cell Calcium.* **12**, 87–95.

Cohen, D. S., J. C. Neu and R. R. Rosales. 1978. Rotating spiral wave solutions of reaction–diffusion equations. *SIAM J. appl. Math.* **35**, 536–547.

Cuthbertson, K. S. R. 1989. Intracellular calcium oscillators, In *Cell to Cell Signaling: From Experiments to Theoretical Models*, A. Goldbeter (Ed.) pp. 435–447. London: Academic Press.

Cuthbertson, K. S. R. and T. R. Chay. 1991. Modelling receptor-controlled intracellular calcium oscillators. *Cell Calcium.* **12**, 97–109.

Dockery, J. D. and J. P. Keener. 1989. Diffusive effects on dispersion in excitable media. *SIAM J. app. Math.* **49**, 539–566.

Doedel, E. 1986. *Software for continuation and bifurcation problems in ordinary differential equations.* California Institute of Technology.

Duffy, M. R., N. F. Britton and J. D. Murray. 1980. Spiral wave solutions of practical reaction-diffusion systems. *SIAM J. appl. Math.* **39**, 8–13.

Dupont, G. and A. Goldbeter. 1989. Theoretical insights into the origin of signal-induced calcium oscillations, In *Cell to Cell Signalling: From Experiments to Theoretical Models*, A. Goldbeter (Ed.), pp. 461–474. London: Academic Press.

Dupont, G., M. J. Berridge and A. Goldbeter. 1991. Signal-induced Ca^{2+} oscillations: properties of a model based on Ca^{2+}-induced Ca^{2+} release. *Cell Calcium.* **12**, 73–85.

Endo, M., M. Tanaka and Y. Ogawa. 1970. Calcium induced release of calcium from the sarcoplasmic reticulum of skinned skeletal muscle fibres. *Nature* **228**, 34–36.

Fabiato, A. 1983. Calcium-induced release of calcium from the cardiac sarcoplasmic reticulum. *Am. J. Physiol.* **245**, C1–C14.

Fabiato, A. and F. Fabiato. 1975. Contractions induced by a calcium-triggered release of calcium from the sarcoplasmic reticulum of single skinned cardiac cells. *J. Physiol.* **249**, 469–495.

Finch, E. A., T. J. Turner and S. M. Goldin. 1991. Calcium as a coagonist of inositol 1,4,5-trisphosphate-induced calcium release. *Science* **252**, 443–446.

FitzHugh, R. 1961. Impulses and physiological states in theoretical models of nerve membrane. *Biophys. J.* **1**, 445–466.

FitzHugh, R. 1969. Impulses and physiological states in models of nerve membrane. In *Biological Engineering*, H. P. Schwan (Ed.) pp. 1–85. New York: McGraw-Hill.

Gilkey, J. C., L. F. Jaffe, E. B. Ridgway and G. T. Reynolds. 1978. A free calcium wave traverses the activating egg of the medaka *oryzias latipes*. *J. Cell Biol.* **76**, 448–466.

Girard, S., A. Luckhoff, J. Lechleiter, J. Sneyd and D. Clapham. 1992. Two-dimensional model of calcium waves reproduces the patterns observed in *Xenopus* oocytes *Biophys. J.* **61**, 509–517.

Goldbeter, A., G. Dupont and M. J. Berridge. 1990. Minimal model for signal-induced Ca^{2+} oscillations and for their frequency encoding through protein phosphorylation, *Proc. natn. Acad. Sci.* **87**, 1461–1465.

Hagan, P. S. 1982. Spiral waves in reaction–diffusion equations. *SIAM J. appl. Math.* **42**, 762–786.

Harootunian, A. T., J. P. Y. Kao, S. Paranjape., S. R. Adams, B. V. L. Potter, and R. Y. Tsien. 1991. Cytosolic Ca^{2+} oscillations in REF52 fibroblasts: Ca^{2+}-stimulated IP_3 production or voltage-dependent Ca^{2+} channels as key positive feedback elements. *Cell Calcium* **12**, 153–164.

Hastings, S. P. 1974. The existence of periodic solutions to Nagumo's equation. *Q. J. Math.* **25**, 369–378.

Hastings, S. P. 1976. On the existence of homoclinic and periodic orbits for the FitzHugh-Nagumo equations. *Q. J. Math.* **27**, 123–134.

Iino, M. 1990. Biphasic Ca^{2+} dependence of inositol 1,4,5-trisphosphate-induced Ca^{2+} release in smooth muscle cells of the Guinea Pig *Taenia Caeci*. *J. gen. Physiol.* **95**, 1103–1122.

Jacob, R. 1991. Calcium oscillations in endothelial cells. *Cell Calcium* **12**, 127–134.

Keener, J. P. 1980. Waves in excitable media. *SIAM J. appl. Math.* **39**, 528–548.

Keener, J. P. 1986. A geometrical theory for spiral waves in excitable media. *SIAM J. appl. Math.* **46**, 1039–1056.

Kopell, N. and L. N. Howard. 1973. Plane wave solutions to reaction-diffusion equations. *Stud. appl. Math.* **52**, 291–328.

Kopell, N. and L. N. Howard. 1981. Target pattern and spiral solutions to reaction–diffusion equations with more than one space dimension. *Adv. Appl. Math.* **2**, 417–449.

Kuba, K. and S. Takeshita. 1981. Simulation of intracellular Ca^{2+} oscillation in a sympathetic neurone. *J. theor. Biol.* **93**, 1009–1031.

Lane, D. C., J. D. Murray and V. S. Manoranjan. 1987. Analysis of wave phenomena in a morphogenetic mechanochemical model and an application to post-fertilization waves on eggs. *IMA J. Math. appl. Med. Biol.* **4**, 309–331.

Lechleiter, J., S. Girard, D. Clapham and E. Peralta. 1991a. Subcellular patterns of calcium release determined by G protein-specific residues of muscarinic receptors. *Nature* **350**, 505–508.

Lechleiter, J., S. Girard, E. Peralta and D. Clapham. 1991b. Spiral calcium wave propagation and annihilation in *Xenopus laevis* oocytes. *Science* **252**, 123–126.

McKean, H. P. 1970. Nagumo's equation. *Adv. Math.* **4**, 209–223.

Maginu, K. 1985. Geometrical characteristics associated with stability and bifurcations of periodic travelling waves in reaction-diffusion equations. *SIAM J. appl. Math.* **45**, 750–774.

Meyer, T. and L. Stryer. 1988. Molecular model for receptor-stimulated calcium spiking. *Proc. natn. Acad. Sci.* **85**, 5051–5055.

Murray, J. D. 1989. *Mathematical Biology*. Berlin: Springer-Verlag.

Murray, J. D. and G. F. Oster. 1984. Generation of biological pattern and form. *IMA J. Math. appl. Med. Biol.* **1**, 51–75.

Neu, J. C. 1979. Chemical waves and the diffusive coupling of limit cycle oscillators. *SIAM J. appl Math.* **36**, 509–515.

Oster, G. F. and G. M. Odell. 1984. Mechanics of cytogels I: oscillations in Physarum. *Cell Motility* **4**, 469–503.

Parker, I. and I. Ivorra. 1990. Inhibition by Ca^{2+} of inositol trisphosphate-mediated Ca^{2+} liberation: a possible mechanism for oscillatory release of Ca^{2+}. *Proc. natn. Acad. Sci.* **87**, 260–264.

Peskin, C. S. 1976. *Partial Differential Equations in Biology.* New York: Courant Insitute of Mathematical Sciences, New York University.

Petersen, O. H., D. V. Gallacher, M. Wakui, D. I. Yule, C. C. H. Petersen and E. C. Toescu. 1991. Receptor-activated cytoplasmic Ca^{2+} oscillations in pancreatic acinar cells: generation and spreading of Ca^{2+} signals. *Cell Calcium* **12**, 135–144.

Rinzel, J. 1976. Simple model equations for active nerve conduction and passive neuronal integration. *Lect. Math. Life Sci.* **8**, 125–164.

Rinzel, J. and J. B. Keller. 1973. Traveling wave solutions of a nerve conduction equation. *Biophys J.* **13**, 1313–1337.

Sanderson, M. J., A. C. Charles and E. R. Dirksen. 1990. Mechanical stimulation and intercellular communication increases intracellular Ca^{2+} in epithelial cells. *Cell Regulat.* **1**, 585–596.

Sauvé, R., A. Diarra, M. Chahine, C. Simoneau, N. Morier and G. Roy. 1991. Ca^{2+} oscillations induced by histamine H_1 receptor stimulation in HeLa cells: Fura-2 and patch clamp analysis. *Cell Calcium.* **12**, 165–176.

Swillens, S. and D. Mercan. 1990. Computer simulation of a cytosolic calcium oscillator. *Biochem. J.* **271**, 835–838.

Thomas, A. P., D. C. Renard and T. A. Rooney. 1991. Spatial and temporal organization of calcium signalling in hepatocytes. *Cell Calcium* **12**, 111–126.

Troy, W. C. 1976. Bifurcation phenomena in FitzHugh's nerve conduction equations. *J. Math. analys. appl.* **54**, 678–690.

Tsien, R. W. and R. Y. Tsien. 1990. Calcium channels, stores, and oscillations. *A. Rev. Cell Biol.* **6**, 715–760.

Tsunoda, Y. 1991. Oscillatory Ca^{2+} signaling and its cellular function. *The New Biol.* **3**, 3–17.

Zykov, V. S. 1980. Analytic evaluation of the dependence of the speed of excitation wave in a two-dimensional excitable medium on the curvature of its front. *Biophys.* **25**, 906–911.